ELSEVIER

Journal of Nuclear Materials 241–243 (1997) 782–787

journal of nuclear materials

Local impurity puffing as a scrape-off layer diagnostic on the Alcator C-Mod tokamak

D. Jablonski, B. LaBombard *, G.M. McCracken, S. Lisgo [1], B. Lipschultz, I.H. Hutchinson, J. Terry, P.C. Stangeby [1]

Plasma Fusion Center, Massachusetts Institute of Technology, Cambridge, MA 02139, USA

Abstract

A capillary injection system has been installed on Alcator C-Mod which allows the localized introduction of gaseous species at a variety of poloidal locations. An experimental program has been undertaken to observe impurity puffs with a CCD camera through appropriate optical filters. The comet-like shape of an ion line emission plume formed in the region of an injection graphically displays the direction of background deuterium flow as well as that of the poloidal impurity ion drift. Parallel and cross-field one-dimensional fluid models are used to characterize the plume shapes and to deduce the background plasma temperature, the parallel flow velocity and the poloidal drift velocity of the impurity ion. Model results are benchmarked against simulations of DIVIMP, a Monte Carlo code, and fast scanning probe measurements. The experiments present a novel diagnostic technique to elucidate local edge impurity transport.

Keywords: Alcator C-Mod; SOL plasma; Impurity transport; Plasma flow diagnostic

1. Introduction

Observing the line emission patterns formed in the region of the scrape-off layer (SOL) of an impurity puff provides unique opportunities for investigation of impurity transport as well as diagnosis of the background plasma. The experiments on Alcator C-Mod [1] have involved imaging plumes at a range of poloidal locations in a variety of plasma discharges, with both lower and upper X-point configurations, and in normal and reversed field directions. This paper discusses general observations, focusing on analysis of the first-charge-state plumes formed at the inner-wall midplane viewed from the outboard.

Plumes have been observed and modeled on other machines employing two methods: the use of a complex fluid or Monte Carlo code, as was done by Matthews et al. [2], McCracken et al. [3], and Pitcher et al. [4], and the use of simple analytic model based coulomb collision and ionization relations, as was done by Pitcher [5]. An intermediate approach has been taken in this work, namely, numerically solving a simplified 1D fluid model which retains coupled continuity, momentum and energy equations. A benefit of this method is the potential to analyze a large number of images in relatively short order, allowing the technique to be used as a regular diagnostic. The efficacy of this fluid paradigm is evaluated by comparison with calculations of DIVIMP [6], a Monte Carlo code, and with measurements of the fast scanning probe [7].

2. Experiments

The primary tools for the experiments are shown in Fig. 1. The neutral gas injection array (NINJA) is a capillary puffing system which can deliver gaseous species at 20 poloidal and 5 toroidal locations [8]. Puff locations discussed below are labeled A, B, and C for reference. Line emission patterns produced in the vicinity of the capillary outlets are imaged from two viewpoints (marked on Fig. 1) by CCD cameras with selectable optical interference bandpass filters (typical bandwidth of 1–20 nm). Filters are chosen to select bright impurity lines in parts of the spectrum where no significant overlap from other lines occurs. The cameras are located outside the vessel, with coherent fiber bundles leading to a standard camera lens at

* Corresponding author. Tel.: +1-617 253 6942; fax: +1-617 253 0627.

[1] University of Toronto IAS, Toronto, Canada M3H 5T6.

PII S0022-3115(96)00606-X

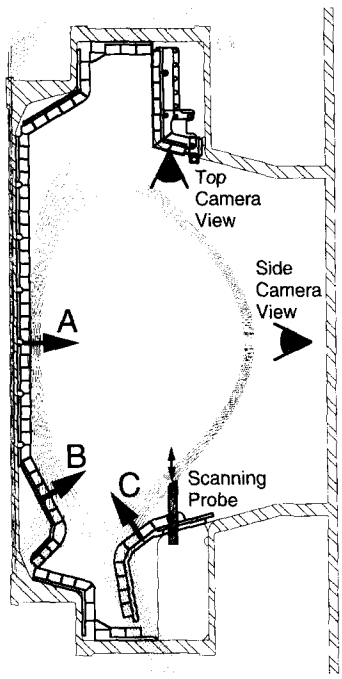

Fig. 1. Layout of plume experiments on the Alcator C-Mod tokamak: the capillary puff locations utilized in the experiments discussed are marked with arrows and labeled for reference; eyes indicate the CCD camera views; the fast scanning probe poloidal location and trajectory are shown.

the view. The cameras are controlled with multiple automatic camera exposure control and display (MACECAD) units [9]. Profile measurements of density, electron temperature, floating potential, and parallel flow velocity in the SOL are provided by the fast scanning probe at the poloidal location shown in the figure. All of the experiments were performed in 0.8 MA, 5.3 T on axis, single-null diverted discharges. Data were taken during the steady-state portion of the discharges with maintenance gas fueling only (at outer midplane) and no divertor pumping.

The shape of the ion plumes observed is typically comet-like, with a tail extending along the field line towards the nearest strike-point. An example of this is shown in Fig. 2. For this lower X-point shot, nitrogen is puffed simultaneously at the inner and outer divertors (locations B and C) while viewed with the top camera through an N-II (463 nm) filter. The tail of each plume is directed towards the nearest strike-point, CCW viewed from the top at the outer divertor and CW at the inner. This behavior is observed for both the first and second ionization states, regardless of $\boldsymbol{B} \times \nabla B$ direction and X-point location. Fig. 3 shows contour plots of C-II (515 nm) brightness during methane gas puffs at the inner midplane (location A) observed with the side camera in upper and lower X-point shots with $\boldsymbol{B} \times \nabla B$ pointing downwards. In both cases, the parallel flow is directed towards the nearest strike point.

Work has focused on the inner-wall midplane because of the excellent view accorded by the side camera, and because the geometry and transport can be easily unfolded. Neutral emission observed for He-I (588 nm) during helium injection is seen to be circular in shape, approximately Gaussian in profile with a FWHM of 3.5 cm around the injection site. The emission profiles from ions, as mentioned above, are asymmetric. This asymmetry is attributed to Coulomb collisions with flowing background deuterium. A local radiative cooling effect cannot explain the asymmetry due to the observation that the plume shape does not alter with a change in gas injection rate. Asymmetry in the emission profiles are also seen in the cross-field

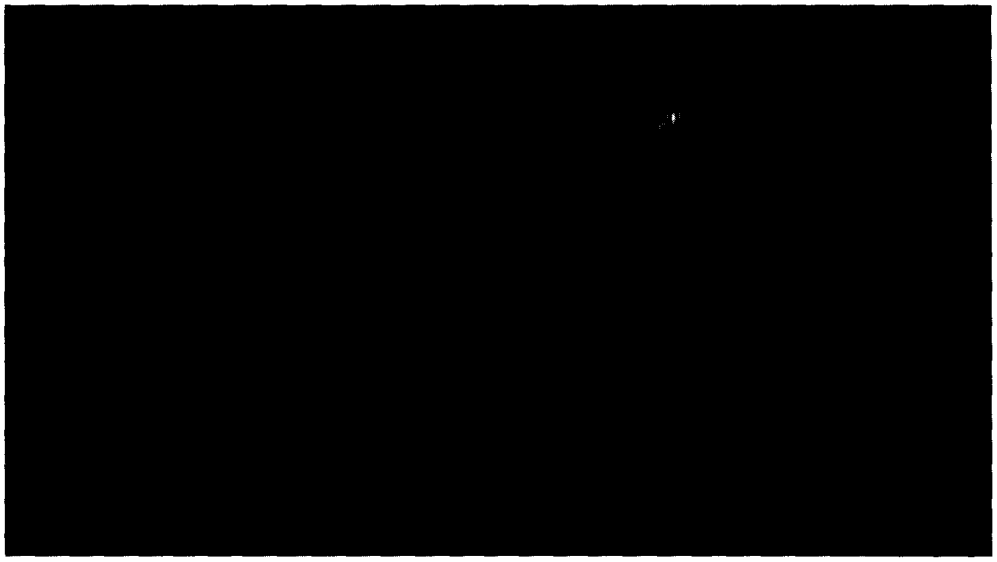

Fig. 2. Top camera view through N-II filter of simultaneous nitrogen puffs at inner and outer divertor (locations B and C). The tail of each plume extends along the field line towards the nearest strike-point.

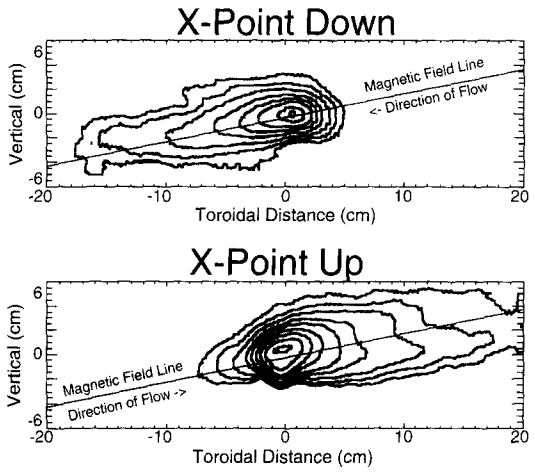

Fig. 3. Contour plots of images of methane puffs at inner-wall midplane (location A) viewed by side camera through a C-II filter in lower and upper X-point discharges (origin corresponds to the gas injection location); background deuterium ion flow is indicated towards the nearest strike-point in both shots.

direction, providing evidence of perpendicular transport. In shots with a downward $\boldsymbol{B} \times \nabla B$ direction, the plumes are seen to have upward deviations from the field line, indicating poloidally upward impurity ion drift. Similarly, the plumes display a downwards deviation when the direction of B is reversed.

3. Model

Emission profiles parallel and perpendicular to the magnetic field are obtained by integrating the two-dimensional image of the plume across and along the field lines respectively. These profiles are modeled with the fluid equations discussed below. While the impurity ions lack self-collisionality, the high collisionality these ions have with the background deuterium lends validity to the application of local fluid parameters [8]. Analysis is restricted to the first charge state of the impurities.

The parallel transport of the ions is characterized with a set of continuity, momentum, and energy equations (where x is the parallel spatial variable):

$$\frac{\mathrm{d}}{\mathrm{d}x}(nv) = S_n - nn_e\langle\sigma v\rangle_i \tag{1}$$

$$\frac{\mathrm{d}}{\mathrm{d}x}\left(nv^2 + \frac{nT}{m}\right) = n\frac{v_D - v}{\tau_v} - nvn_e\langle\sigma v\rangle_i \tag{2}$$

$$\frac{\mathrm{d}}{\mathrm{d}x}\left(\frac{1}{2}nv^3 + \frac{5}{2}\frac{nT}{m}v\right) = n\frac{T_D - T}{\tau_T} + nv\frac{v_D - v}{\tau_v} - \left(\frac{1}{2}nv^2 + \frac{3}{2}\frac{nT}{m}\right)n_e\langle\sigma v\rangle_i \tag{3}$$

for which unscripted variables represent impurity ion parameters, n_e the electron density, T_D and v_D the background plasma temperature and parallel velocity, and $\langle\sigma v\rangle_i$ the rate coefficients of the ionization to the next charge state. The appropriate coefficients given by Bell et al. [10] are used. The background deuterium and electron temperatures are assumed to be equal. The particle source term, S_n, constitutes ionization from the neutral state. Presently, its shape for all injected gases is taken as that of the observed neutral He-I emission profiles (Gaussian, FWHM of 3.5 cm, centered at $x = 0$). In future experiments, this approximation for nitrogen and methane source profiles will be improved both by direct measurement of the N-I and C-I emission patterns and by consideration of molecular ionization effects. The characteristic momentum (τ_v) and energy (τ_T) equilibration times given by Spitzer [11] are employed to account for Coulomb collisions with the background plasma. The background plasma values are taken as constant. Three inputs are needed (n_e, T_D, and v_D) to solve the equations for the three outputs (profiles of impurity ion n, T, and v). Boundary conditions at $x = \pm\infty$ of $n = 0$, $\mathrm{d}T/\mathrm{d}x = 0$ and $\mathrm{d}v/\mathrm{d}x = 0$ are employed using a coordinate transformation.

The inverse problem is actually the one in which we are most interested, namely, input the impurity ion profile, n, and determine the background plasma parameters, n_e, T_D, and v_D. In the experiments outlined below, the experimentally observed emission profile shapes are matched with modeled impurity density profiles by specifying the electron density, n_e (provided by scanning probe measurements), and determining the background plasma temperature and deuterium ion velocity that provide the best fit.

The perpendicular behavior of the ions is characterized with a continuity equation (where z is the spatial variable):

$$-D\frac{\mathrm{d}^2 n}{\mathrm{d}z^2} + v\frac{\mathrm{d}n}{\mathrm{d}z} + n_e\langle\sigma v\rangle_i n = S_o e^{-(z/\lambda)^2} \tag{4}$$

where D and v are the poloidal diffusion coefficient and drift velocity respectively. The Gaussian form of the particle source has been inserted (with $\lambda = 2$ cm). Assuming D and v are constant, this equation can be solved analytically in terms of error functions. Because the characteristic diffusion lengths are much smaller than the width of the source, the solutions are insensitive to the value of D employed. To match a given perpendicular profile, the density (provided by the scanning probe), temperature (found as a solution from the parallel transport equations), and diffusion coefficient are taken as given, and the value of poloidal drift velocity which provides the best fit is found. In summary, for a given two-dimensional plume and specified electron density, Eqs. (1)–(4) are used to find the background plasma temperature, the background deuterium parallel velocity, and the impurity ion poloidal drift velocity.

DIVIMP (divertor impurities), a three dimensional edge

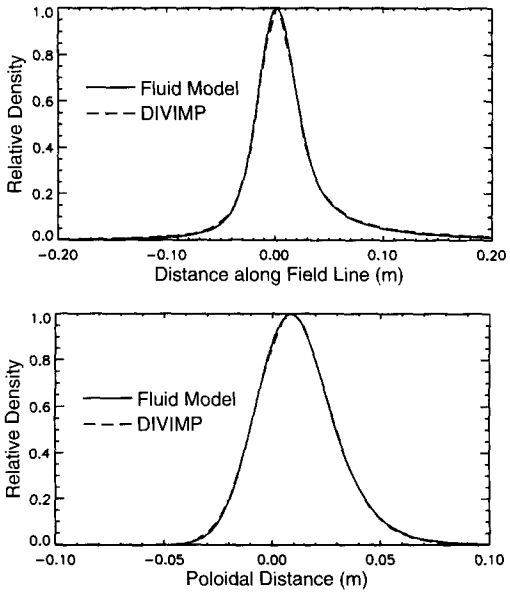

Fig. 4. Best fluid model fits to integrated parallel and perpendicular profiles of C-II plume produced by DIVIMP. DIVIMP utilizes typical C-Mod edge profiles of density and temperature. Using the electron density at the radial location where DIVIMP has C-II ions peaked, the fluid model fits a temperature of 16.2 eV (compared with 17 eV at the flux surface of the employed density), a parallel deuterium flow velocity of 12400 m/s (13000 input to DIVIMP), and an impurity ion drift of 1800 m/s (1500 input to DIVIMP).

impurity transport Monte Carlo code, is used to benchmark the model. DIVIMP accounts for phenomena not covered by the fluid equations, namely partial collisionality and three-dimensional aspects of impurity transport. Further, the comparison provides an independent check of the numerical solutions. The results of one such comparison are shown in Fig. 4. For this case, typical edge density and temperature radial profiles, a parallel deuterium velocity of 13000 m/s, and a poloidal impurity ion drift of 1500 m/s are modeled to produce a plume which is integrated to obtain the parallel and perpendicular profiles. Using the plasma density at the radial location where DIVIMP gives the C-II density as peaked (n_e of 2.3×10^{19} m^{-3}), the best fluid model fits are shown in the figure. The resultant temperature, 16.2 eV, compares with 17 eV at the radial location where C-II is peaked. The fluid model derived parallel and poloidal velocity values of 12400 and 1800 m/s are within 5 and 15% of the DVIMP modeled values respectively.

4. Results

An example of the fluid analysis for an experimental plume is shown in Fig. 5. This plume was observed in a lower X-point discharge with a core volume averaged electron density ($\bar{n}_e$) of 2.1×10^{20} m^{-3}. The electron density measured by the scanning probe at the appropriate flux surface is employed (5.6×10^{19} m^{-3}). While the scanning probe and plume are at different poloidal locations (see Fig. 1), one expects plasma pressure outside of the divertor region to be conserved along a field line, meaning that if the plume derived temperature matches that measured by the scanning probe, the accuracy of the density used by the model for the inner-wall puff location is verified. The temperature found with the parallel solution, 10.2 eV, does show agreement with that of the scanning probe (9.5 eV). A parallel deuterium Mach number of 0.4 (towards the lower divertor) and a poloidal impurity ion drift of 365 m/s (upward) are found. If this drift is due to $\boldsymbol{E} \times \boldsymbol{B}$, a radially outward electric field would be estimated as 2920 V/m.

Error analysis shows the uncertainty of resultant temperature and poloidal drift to be relatively small. Uncertainty in the temperature, primarily due to possible error in the employed density, is 10% or less, and uncertainty in the drift velocity, primarily due to uncertainty in the ionization rate coefficients used by the model, is on the order of 20%. For Mach number, the accuracy of the assumed density is critical. Roughly speaking, the Mach number will be known only as well as is the electron density at the plume location.

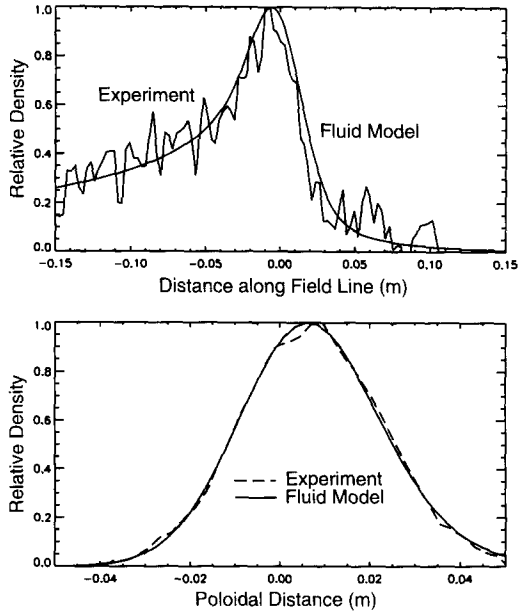

Fig. 5. Best fluid model fits to integrated profiles of an inner-wall midplane (location A) N-II plume viewed by the side camera. Using the electron density measured by the scanning probe at the appropriate flux surface, the model fits to a temperature of 10.2 eV (compared with 9.5 eV measured by the scanning probe), a Mach number of 0.4, and a poloidal impurity ion drift of 365 m/s.

Table 1
Plume and fast scanning probe measurement comparison for a series of discharges

Core n_e ($\times 10^{20}$ m^{-3})	Species	Temperature (eV)		Mach number		E_r-field (V/m)	
		plume	FSP	plume	FSP	plume	FSP
1.5	N-II	7.5	8.0	0.20	−0.44	1360	1100
2.1	N-II	10.0	9.5	0.35	−0.32	2190	1900
2.1	N-II	10.0	9.5	0.40	−0.36	2920	1500
2.3	He-II	17.0	15.5	0.15	−0.20	1080	3700
1.7	He-II	20.0	20.5	0.25	−0.14	420	5000
1.2	N-II	8.0	8.0	0.25	−0.36	520	1500

While the temperature comparison should be viewed quantitatively, comparisons of Mach number and radial electric field are meant to be qualitative (since measurements are made at different poloidal locations).

Parameters derived from plume analysis for a series of discharges are compared with scanning probe measurements in Table 1. All of the shots had lower X-points. The values of n_e, along with the measurements of temperature, Mach number, and electric field are listed. Fast scanning probe Mach numbers are derived from the ratio of upstream to downstream ion saturation current using the Hutchinson formulation, which sets momentum and particle diffusivities equal in its derivation of the appropriate fluid equations [12]. Radial electric fields at the scanning probe location are calculated by taking the derivative of the plasma potential derived from standard Langmuir probe theory.

While the temperature comparison in the table is a quantitative one, the Mach number and electric field comparisons should be viewed qualitatively. Excellent temperature agreement is shown in the third and fourth columns, validating the model use of the scanning probe measured electron density. The scanning probe measurements of Mach number indicate the order of magnitude of flow velocity one would expect in the C-Mod SOL. Mach numbers obtained from both the plumes and the probe range between 0.1 and 0.5. The negative values for the scanning probe measurements indicate flow towards the outer strike point (as opposed to the flow towards the inner strike-point indicated at the inner-wall). Electric field values on the order of 10^3 V/m are seen by both measurements. The observation that electric fields derived from plume analysis and scanning probe measurements are often much different is understood, both because different values are expected at the two locations, and because the uncertainty of the calculated electric field at the scanning probe is about 50%.

5. Conclusions

These experiments have demonstrated that the technique of local impurity puffing and plume analysis can play a unique role in diagnosing the C-Mod SOL. The direction of flow of the background deuterium ions and the direction of the impurity ion drift are clearly seen in the raw experimental data. This on its own is of value because of the great flexibility and ease of use of the technique. Plumes can be observed wherever a capillary puff location with a view available of it is located. A relatively simple fluid model can be used to determine the background plasma temperature, parallel flow velocity, and impurity ion poloidal drift velocity. The model paradigm has been shown valid through quantitative comparisons with DIVIMP and scanning probe measured temperatures, and qualitative comparisons with scanning probe measurements of Mach number and electric field. With a more complete system, the local plasma density could also in principle be extracted with this technique.

Acknowledgements

The authors would like to express their gratitude to Bob Childs and Tom Toland for their work in construction and implementation of NINJA, to Aaron Allen for constructing the PC based system which digitizes and archives the plume images, and to the other scientists, engineers, technicians, students, and support staff of the Alcator C-Mod team whose dedicated efforts have made this work possible. This work is supported by the U.S. Department of Energy under contract No. DE-AC02-78ET5103.

References

[1] I.H. Hutchinson, R. Boivin, F. Bombarda et al., Phys. Plasmas 1 (1994) 1511.
[2] G.F. Matthews, D.N. Buchenauer, D.N. Hill et al., 18th Eur. Conf. on Controlled Fusion and Plasma Physics (1990), III-229.
[3] G.M. McCracken, U. Samm, S.J. Fielding et al., J. Nucl. Mater. 176–177 (1990) 191.
[4] C.S. Pitcher, P.C. Stangeby, D.H.J. Goodall et al., J. Nucl. Mater. 162–164 (1989) 337.
[5] C.S. Pitcher, Ph.D. Thesis, University of Toronto IAS (1987).
[6] P.C. Stangeby, C. Farrell, S. Hoskins et al., Nucl. Fusion 28 (1988) 1945.

[7] B. LaBombard, J. Goetz, C. Kurz et al., Phys. Plasmas 2 (1995) 2242.
[8] D. Jablonski, Ph.D. Thesis, MIT Plasma Fusion Center (1996).
[9] D.H.J. Goodall and M.N. Price, J. Nucl. Mater. 196–198 (1992) 1047.
[10] K.L. Bell, H.B. Gilbody, J.G. Hughes et al., Atomic and Molecular Data for Fusion, Part I, UKAEA Report CLM-R216 (1982).
[11] L. Spitzer, Jr., Physics of Fully Ionized Gases (Interscience, New York, 1956).
[12] I.H. Hutchinson, Phys. Fluids 30 (1987) 3777.